CCFE-R(14)23

Mark R. Gilbert, Zamir Ghani and Lee W. Packer

# Optimising the Neutron Environment of Radiation Portal Monitors: a Computational Optimisation Study

# Optimising the Neutron Environment of Radiation Portal Monitors: a Computational Optimisation Study

Mark R. Gilbert, Zamir Ghani and Lee W. Packer

*EURATOM/CCFE Fusion Association, Culham Science Centre, Abingdon, Oxon. OX14 3DB, UK.*

# Optimising the neutron environment of Radiation Portal Monitors: a computational optimisation study

Mark R. Gilbert, Zamir Ghani and Lee W. Packer

*UK Atomic Energy Authority, Culham Science Centre, Abingdon OX14 3DB, UK*

Written in consultation with

John McMillan of Sheffield University and Val O'Shea of Glasgow University

**CONTENTS**

# Optimising the neutron environment of Radiation Portal Monitors: a computational optimisation study

Mark R. Gilbert, Zamir Ghani and Lee W. Packer

*UK Atomic Energy Authority, Culham Science Centre, Abingdon OX14 3DB, UK*

## 1 INTRODUCTION

The CLASP scheme proposal 'Optimising the neutron environment of Radiation Portal Monitors (RPM)' [1], which is a collaboration between Glasgow University (Val O'Shea), Sheffield University (John McMillan) and the UK Atomic Energy Authority was awarded funding through STFC in 2012.

The objective of the work reported here is to provide optimised information regarding the design of RPMs with a focus on computational simulations using radiation transport modelling with modern nuclear data libraries. The aim was to demonstrate that enhancements to a generic RPM model design and surrounding environment can enable a significant reduction in the measured neutron background, and hence lower their detection limit to a 'threat' neutron source. In preliminary work, two environmental neutron-field models were developed to evaluate the detection response for a range of RPM modifications and ground or 'roadway' materials. The basic modifications implemented in the models and subsequent optimisation studies demonstrated that, for the modelling assumptions, materials and geometries implemented, the environmental neutron background can be reduced and, with some shielding/collimation modifications to the RPM, neutron alarm levels can be reduced significantly.

This report describes briefly the preliminary study, to provide background, and then explains, in detail, the modelling and findings from a sequence of parameter optimisation studies that more fully explore the possible RPM modifications in the context of reducing the detection limits to a threat neutron source in an environmental neutron field.

## 2 PRELIMINARY SIMULATIONS

Preliminary simulations were performed to demonstrate the benefit, in terms of detecting a threat neutron source above an alarm level defined via the response to an environmental neutron field, by adding shielding and collimation to 'generic' He-3-based RPMs.

### *2.1 Model Description*

#### 2.1.1 Generic He-3 based RPM model

A pair of basic 'generic' He-3-based detector panels were developed for this study. Each RPM panel consists of an array of 13 one atmosphere He-3 tubes, of length 125 cm and radius 2.52 cm of which 0.1 cm is the stainless steel tank enclosing the helium. The tubes are completely surrounded by polythene. Each polythene sub-unit block is of dimension 12 cm x 9.04 cm. The detection panels are 156 cm in length and 135 cm in height. The two

panels are spaced by a distance of 300 cm. The panels are positioned above a ground material volume, which is 100 cm thick. Ground material options are listed in section 2.2.

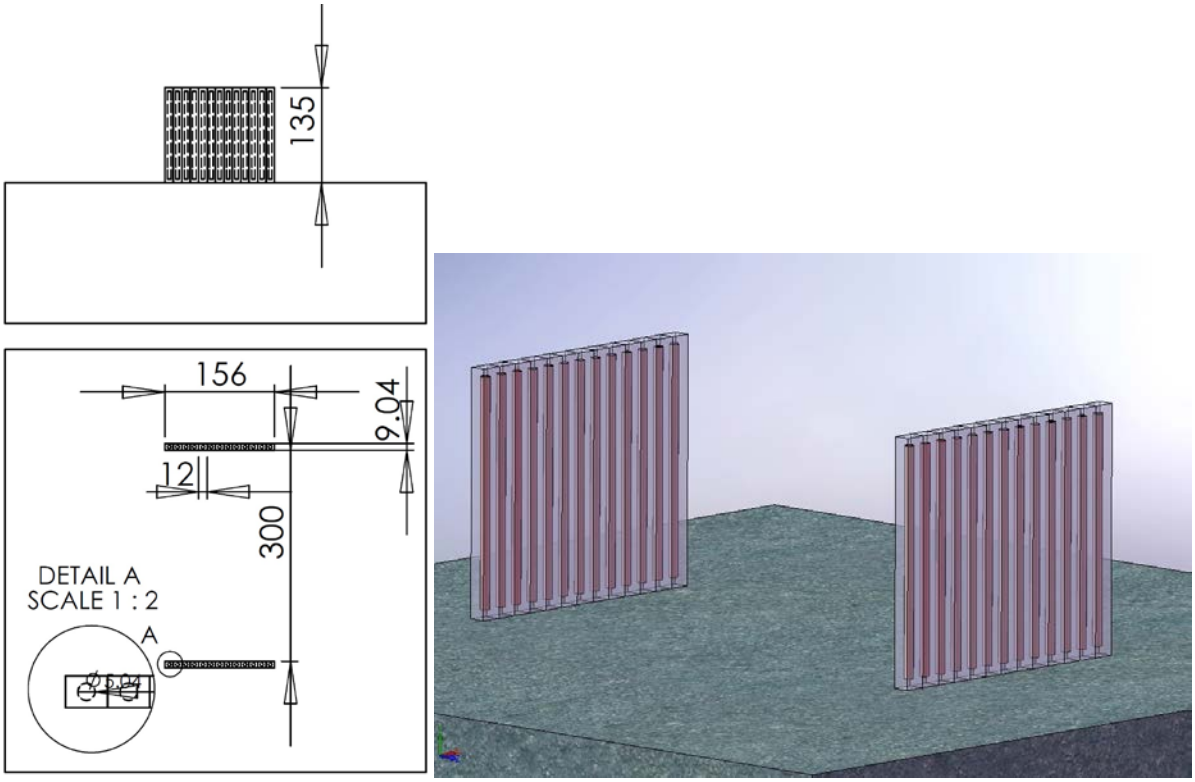


**Figure 1: (lhs) Generic He-3 based panel detector model dimensions (in cm) and 3-D image (rhs).**

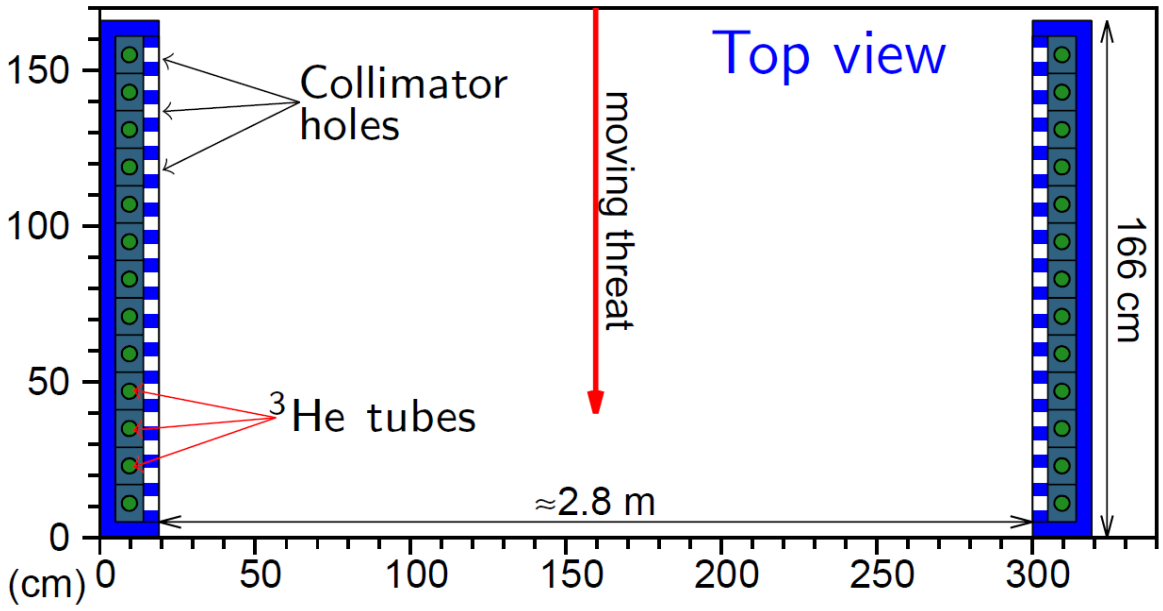


**Figure 2: MCNPX plot of panel model showing 2 panels with 13 He-3 tubes (green regions) surrounded by polythene (grey-blue) and a possible boronated polythene shielding and collimator configuration (blue).**

### 2.1.2 Material definitions

The material definitions shown in Table 1 include all of the various ground materials, as well as the materials used in the model of the detector itself.

**Table 1: Material definitions used in the model**

| | Density g/cc | Reference | Ground material |
|---|---|---|---|
| Polythene | 0.93 | a | N |
| Air | 0.0000541* | a | N |
| He-3 | 0.000025* | a | N |
| 304LN stainless steel | 7.9 | a | Y |
| Asphalt Pavement | 2.5784 | a | Y |
| Blank | 0.0 | - | Y |
| Portland concrete | 2.3 | a | Y |
| Borated silicone rubber (BISCO) – Natual abundance boron | 1.119 | b | Y |
| Borated silicone rubber (BISCO) – enriched to 100% B-10 | 1.119 | Modified from b | Y |
| Water | 1 | - | Y |
| Sea water | 1.023343 | a | Y |
| Borated polythene (nat.) | 1 | a | N |
| Borated polythene (enriched 100% B-10) | 1 | a | N |

*atoms-barn cm units

[a] RJ McConn Jr, Compendium of Material Composition Data for Radiation Transport Modeling, PNNL-15870 Rev. 1, March 2011

[b] MCNP criticality manual

### 2.1.3 Detector model variants: RPM model with shielding and basic collimator

Three additional variants of the basic He-3 detector were developed for the preliminary study:

1. **Detector with shielding.** Borated polythene shielding was added to the sides, top, bottom and back face of the detector (leaving the ‘detection face’ unshielded). The shielding thickness was set to 5 cm.
2. **Detector with shielding and basic collimator option 1.** A basic collimator was added to the ‘detection face’ of each RPM. The collimator plate consists of borated polythene of thickness 5 cm. The collimator holes are cylindrical of diameter 4.6 cm. The collimator hole pitch (spacing) was set to approximately 5.2 cm. See Figure 3 and Figure 4.
3. **Detector with shielding and basic collimator option 2.** As in 2, except the collimator plate consists of pure polythene of thickness 5 cm. See Figure 3 and Figure 4.

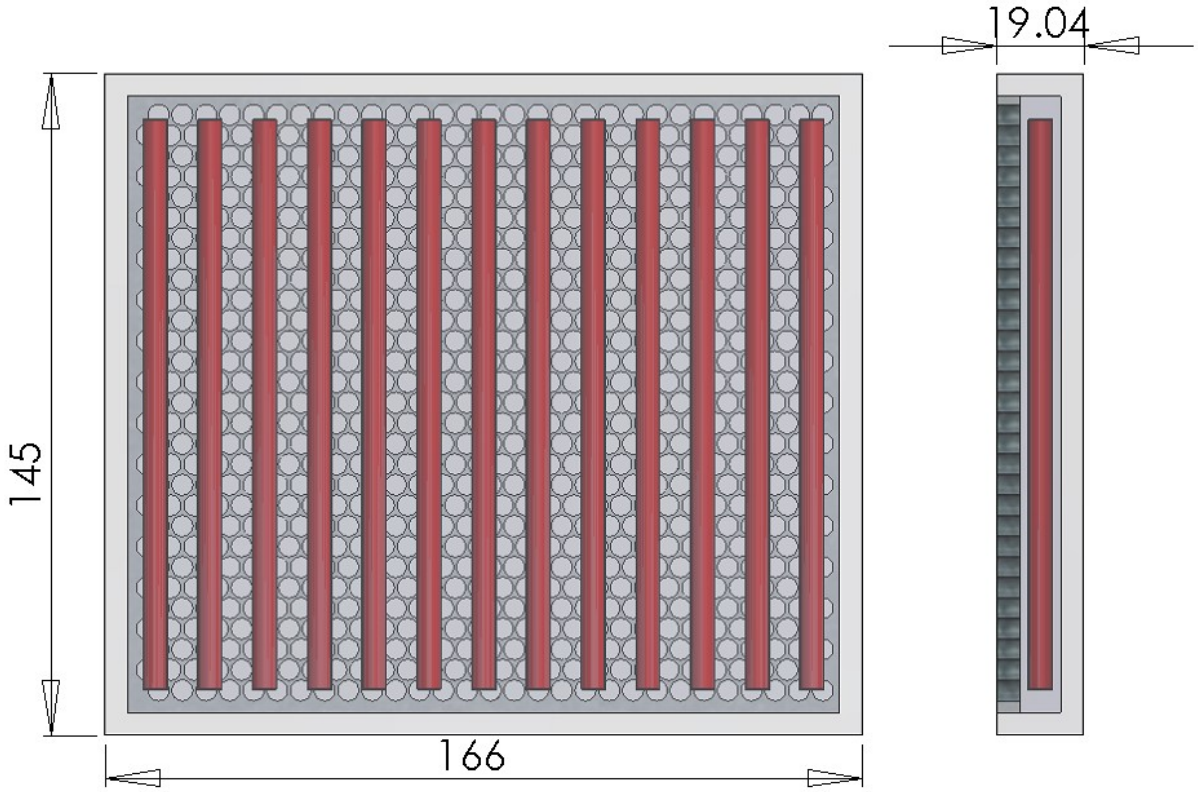


**Figure 3: Dimensions of panel detector with shielding and basic collimator (dimensions in cm).**

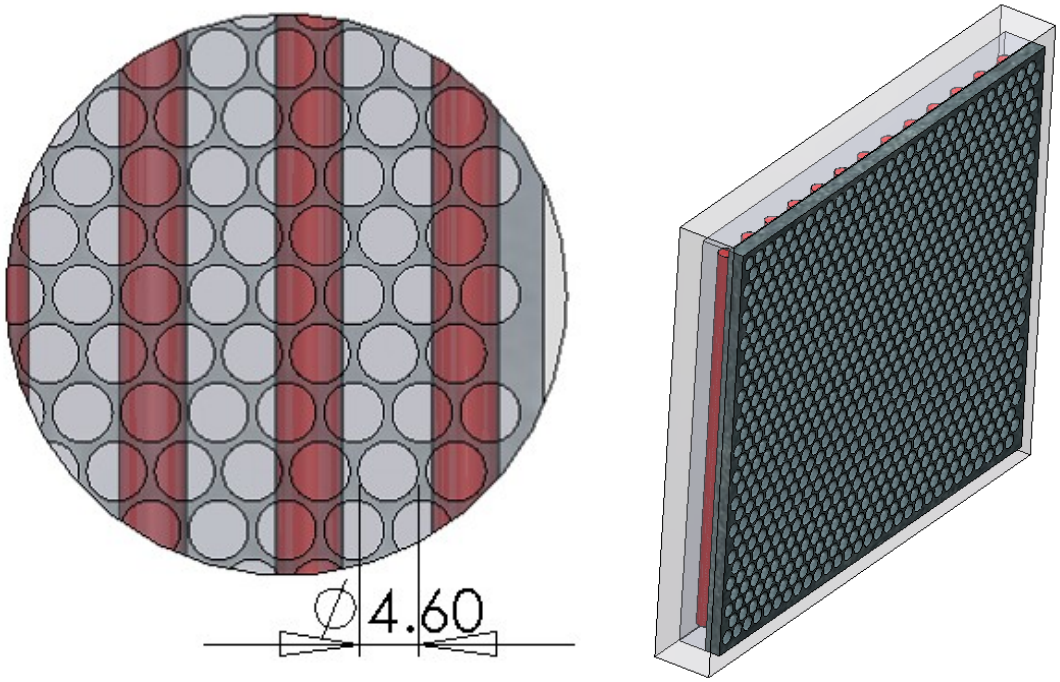


**Figure 4: Collimator hole dimensions in cm (lhs); 3D image of panel detector with collimator panel (rhs)**

### 2.1.4 MCNPX physics model options

MCNPX version 2.7a [2] was used for all calculations presented. The upper neutron energy was adjusted to 1 x $10^5$ MeV (EMAX parameter, phys:N 1E5) with the remaining neutron physics options set as default.

### 2.1.5 Environmental neutron sources

Two neutron spectrum models have been developed:

1. Hemispherical surface source with an isotropic distribution.
2. Planar surface source with a $\cos^2\theta$ distribution from the zenith direction.

The energy spectrum used for both neutron models was derived from EXPACS ver. 2.22 [3]. Input parameters were latitude, 51.0809 and longitude 1.1858 with no environmental parameters. Figure 5 'blank' shows the EXPACS spectrum implemented into the planar surface source model (model 1).

A normalisation factor was calculated for each neutron environment model using the asphalt pavement ground material model and by setting a nominal neutron flux at 100 n $m^2$ $s^{-1}$ [4] in region at the mid-point between the two detectors in this model. This normalisation factor was applied to all other ground material models for comparison and used to general the equivalent He-3 detector response (see Figure 6).

## *2.2 Preliminary simulation results*

Figure 5 shows neutron spectra calculated a spherical region at the midpoint between the two detectors for different ground materials using the planar background source defined in section 2.5. These results demonstrate the significant variation between different ground materials, particularly in how they moderate, or not, the low and high energy parts of the neutron spectrum.

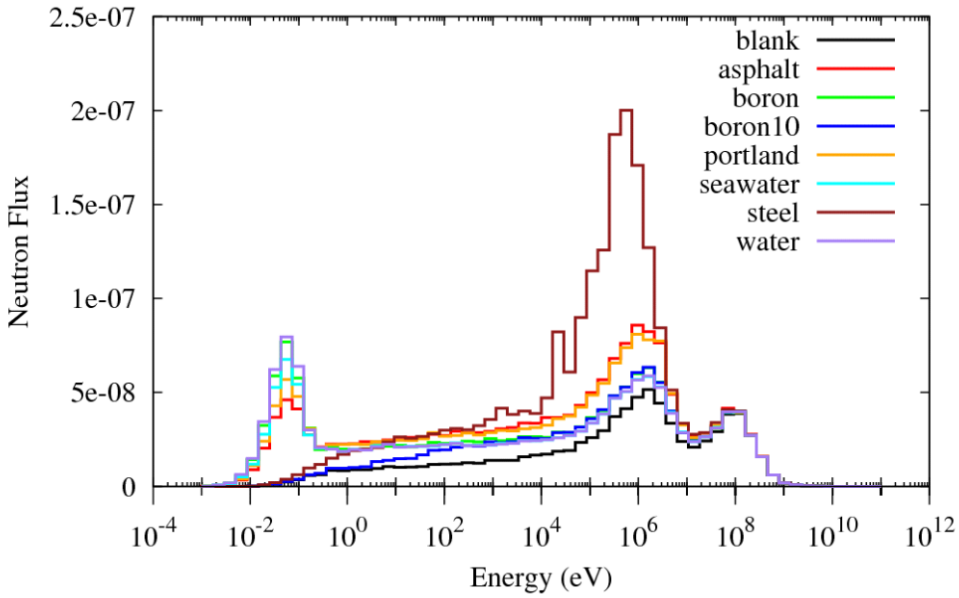


**Figure 5: Comparison of background neutron spectra with different ground materials (planar background source).**

Figure 6 shows a comparison of detector responses to the planar background source for each of the four models developed and for each of the ground materials defined. In the case of the asphalt pavement model the detector background response has been reduced by a factor of 6 from the unshielded RPM and the shielded + collimator option 1 model. It is clear that further reduction in the RPM background response can be achieved by additional choices of the ground material.

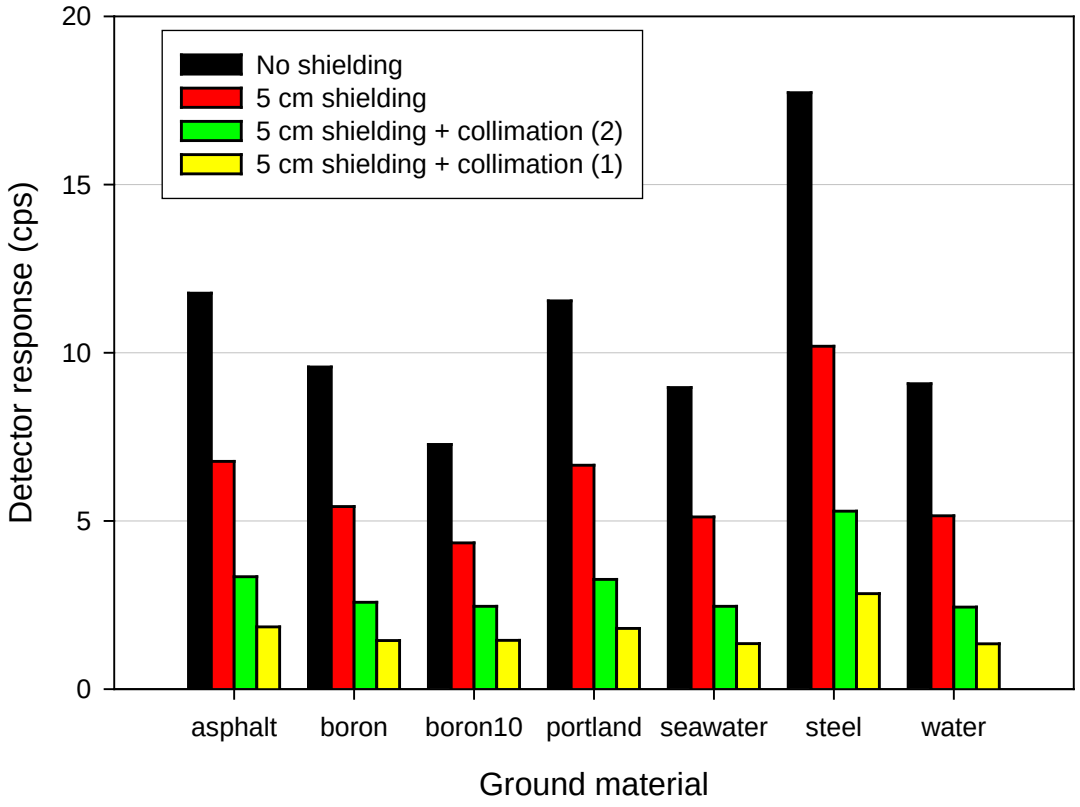


**Figure 6: Comparison of detector responses to environmental neutron background (planar environment source) for unshielded RPM, shielded RPM and shielded RPM with additional front collimator options. Each option is compared against different ground material types.**

Figure 7 shows a comparison of the response of the shielded RPM and shielded + collimator RPM options as a function of $^{252}$Cf neutron source position (emission rate 2 x 10 $^{4}$ n/s) along the x-direction (x=0 is the centre of the detection area between the RPMs) with the asphalt ground material. As expected, the RPM response decreases as x increases, as the source gets further away from the detector. The figure further shows that the collimation geometry defined in the model reduces the RPM response when compared to the shielded non-collimated model. It should be noted that the collimator 2 option (pure polythene) does not exhibit as large a loss of response to the source compared with the collimator 1 option (borated polythene).

To demonstrate the possible practical application of the above findings we integrated the response of each configuration to a threat source moving over asphalt at a typical 2 m/s during a 2 s acquisition time from -2m to +2m (equivalent to integrating the 0-200 cm regions in Figure 7 twice) relative to the middle of the detectors. Alarm levels were set using the Currie limit $B + 4.65\sqrt{B}$ (see section 3.1.1). Results for a threat strength of 2000 n/s are shown in Figure 8. From the figure, we can clearly see that, in this particular scenario, the

unshielded design would not detect the threat, while those with shielding and collimation would.

In collimator designs and material considerations a trade-off exists between 1) achieving a low detector response to the environmental neutron field and 2) minimising the loss of response to a 'threat' source. The optimisation studies later in this report will investigate this trade-off in more detail.

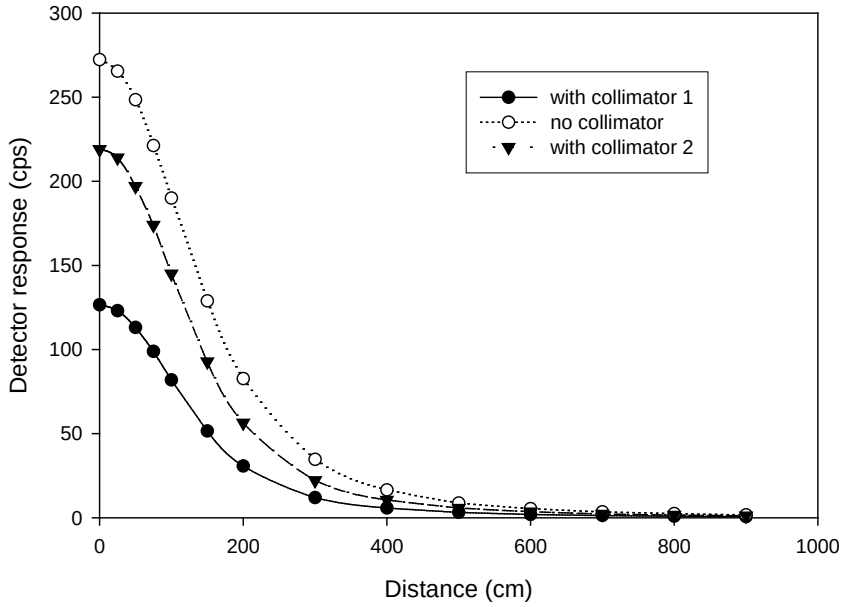


**Figure 7: Comparison of detector responses for collimated options and uncollimated RPMs as a function of distance along the x-direction from the mid-point between the panels (asphalt ground material). Source term is a 2 x $10^4$ n/s emission rate Cf-252 source, and the assumed ground material was asphalt.**

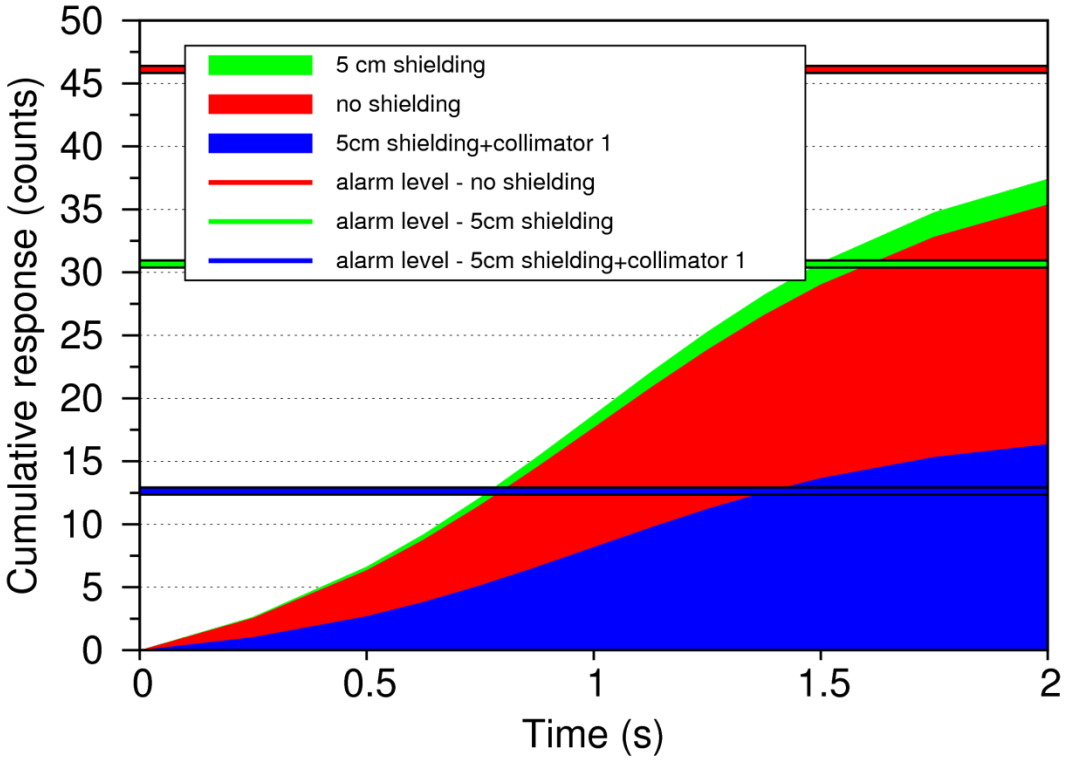


**Figure 8: Source cumulative response over the 2 s acquisition time for the bare, shielded, and shielded with collimator option 1 configurations. The assumed ground material was asphalt**

**and the planar background source was used. The horizontal lines show the associated alarm level for each of the cases.**

# 3 EXTENDED RPM OPTIMISATION STUDY

Having identified that a combination of additional shielding and collimator could improve detector performance, we have performed an extended, parameter study of the RPM design. Parameters that included shielding thickness, as well as collimator depth, profile and packing density have been varied and the resulting detector response compared against an overall system performance function, 'minimum source to alarm' (or `minimum source alarmed' as used in the graphical figures below). The models, calculations and results are described below.

## *3.1 Introduction and terms of extended study*

For this parameter assessment of RPM design we have kept the external variables fixed. In particular, we have used the standard asphalt ground material, which was observed to perform reasonably in the preliminary study discussed above, and a planar background source with a $\cos^2\theta$ angular distribution from the zenith.

### 3.1.1 Performance measure: 'minimum source to alarm'

In a parameter study, a relatively large number of separate responses must be assessed – one for each parameter set – which makes a detailed, counts-vs-time or response-with-position analysis impractical. Thus, for this extended study we have used a single performance measure that can be used to compare different detector configurations.

Firstly, rather than considering the variation in response with the source position (as in Figure 7) we only measure the overall response to a line source representing all possible source positions during the 2s acquisition time. Not only does this reduce the number and complexity of the required Monte-Carlo simulations, but it also means that the threat source response for a given configuration is a well-defined function of a single quantity extracted directly from the MCNPX simulations. The source response, in counts per acquisition $C$ is given by:

$$C = \phi_{src} R_{src} t V_{He},$$

where $\phi_{src}$ is the threat source emission strength with units of n/s (neutrons per second), $R_{src}$ is the (*n,p*) reaction rate (measured by MCNPX) in the helium tubes (reactions per cm$^3$ per neutron), $t$ is the total acquisition time (2s), and $V_{He}$ is the total helium volume in the detector tubes (cm$^3$).

A second Monte-Carlo simulation gives the response of the detector to the planar background, again as an (*n,p*) reaction rate $R_{bkgrd}$, which is used to define an 'Alarm-level' $A$ via the Currie[5] detection limit:

$$A = C_{bkgrd} + 4.65\sigma_{bkgrd},$$

where $\sigma_{bkgrd}$ is the standard deviation of the background count $C_{bkgrd}$ in 2s, which is defined via

$$C_{bkgrd} = N_{bkgrd} R_{bkgrd} t V_{He}.$$

$N_{bkgrd}$ is the background normalisation factor, as discussed in section 2.1.5. To define the relative effectiveness of a particular detector configuration, we then define the 'minimum

source to alarm' as the lowest theoretically detectable threat strength $\phi_{src}^{min}$ by equating $C = A$, using the square root of $C_{bkgrd}$ for $\sigma_{bkgrd}$, and rearranging. For comparison, note that the values of this performance measure for the configurations considered in the preliminary study (with asphalt ground material) are 2638 n/s for the bare, unshielded system, 1647 n/s for the system with 5 cm of boronated polythene behind and at the sides of the detector (which remains fixed for the entire parameter study below), and 1286 n/s for the shielded detector with the 5 cm thick collimator made of boronated polythene (option 1).

### *3.2 Multi-parameter study of shielding and collimation parameters*

Schematics of the detector geometry used for this optimisation study are shown in Figure 9 and Figure 10. Note that here we have taken advantage of the problem symmetry and have only modelled a single detector, locating a reflecting plane on the other side of the source line distribution (see previous section). This simplification not only makes the input file for the MCNP model easier to manipulate and adjust for different parameter sets, but it also reduces computational time, which, as already noted, is crucial when a large number of simulations are required.

In Figure 9 the basic detector design is shown and two of the variable parameters are labelled. The first of these is the collimator depth $\delta$, which varies from 0.1 to 40 cm. In the preliminary study the shielding surrounding the helium tubes was kept fixed with the collimator added on top of this (additional shielding behind the detector, relative to the source, was also added – see Figure 2), but for the optimisation study we allow for extra shielding of thickness $\kappa$ between the detector tubes and collimator, where $\kappa$ ranges from 0 to 10 cm. Note that the material used for this extra shielding is the same basic polythene that surrounds the helium tubes, and is not the boronated polythene used for the collimator and other shielding.

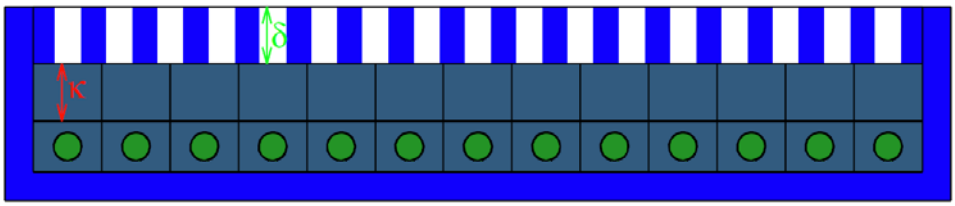


**Figure 9: Top view slice of the single detector configuration used in optimisation study, showing variable parameters δ (collimator depth) and κ (front shielding thickness). In this picture the threat neutrons come from above.**

Two other parameters were considered in the study. The first of these, illustrated by Figure 10, is the profile of the holes in the collimator. In the preliminary study, these were simple cylindrical holes, which could be easily drilled into a sheet of the boronated polythene used to construct the collimator. For the parameter study, the cross sectional profile of the holes was varied using the ratio $i_r/o_r$, where $i_r$ and $o_r$ are the inner (middle) and outer radii of the hole, respectively. This allowed the profile to vary from cylindrical ($i_r/o_r$=1), to progressively more conical profiles (as illustrated in the figure), where $i_r/o_r$ is less than one.

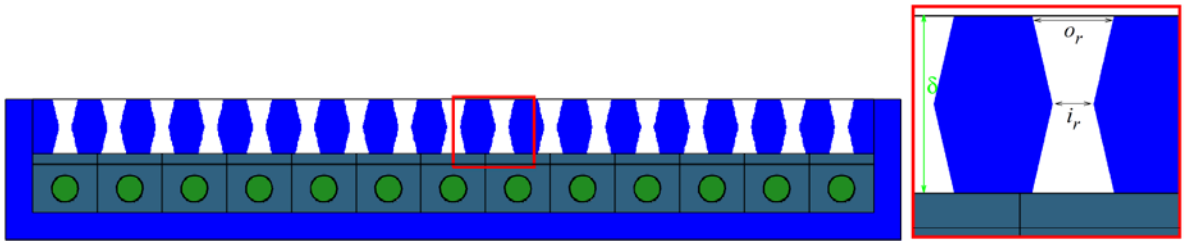


**Figure 10: Top view slice of the detector showing optimisation parameters for collimator profile.**

The final parameter was the packing density of the collimator holes, varied by changing $o_r$ and measured as the percentage open area on the front face of collimator.

### 3.2.1 Results

The initial approach to the parameter study was to allow all of the parameters to vary at the same time, but it quickly became apparent that this made meaningful conclusions difficult. In particular, there is one too many parameters (four) to consider the variation at the graphical level. Thus, we began by optimising the additional shielding thickness $\kappa$, in conjunction with collimator depth $\delta$. From Figure 11, which shows how the minimum detectable threat varies with $\delta$ for various choices of $\kappa$, we see that there is an optimum at 1-2 cm for this extra shielding, under the assumption that the collimator depth is close to optimum. Note that, for very thick collimators, sufficient attenuation is achieved without the need for extra shielding, and so $\kappa = 0$ is optimal (red curve in figure). However, very large $\delta$ are not likely as these do not produce good overall detector performance.

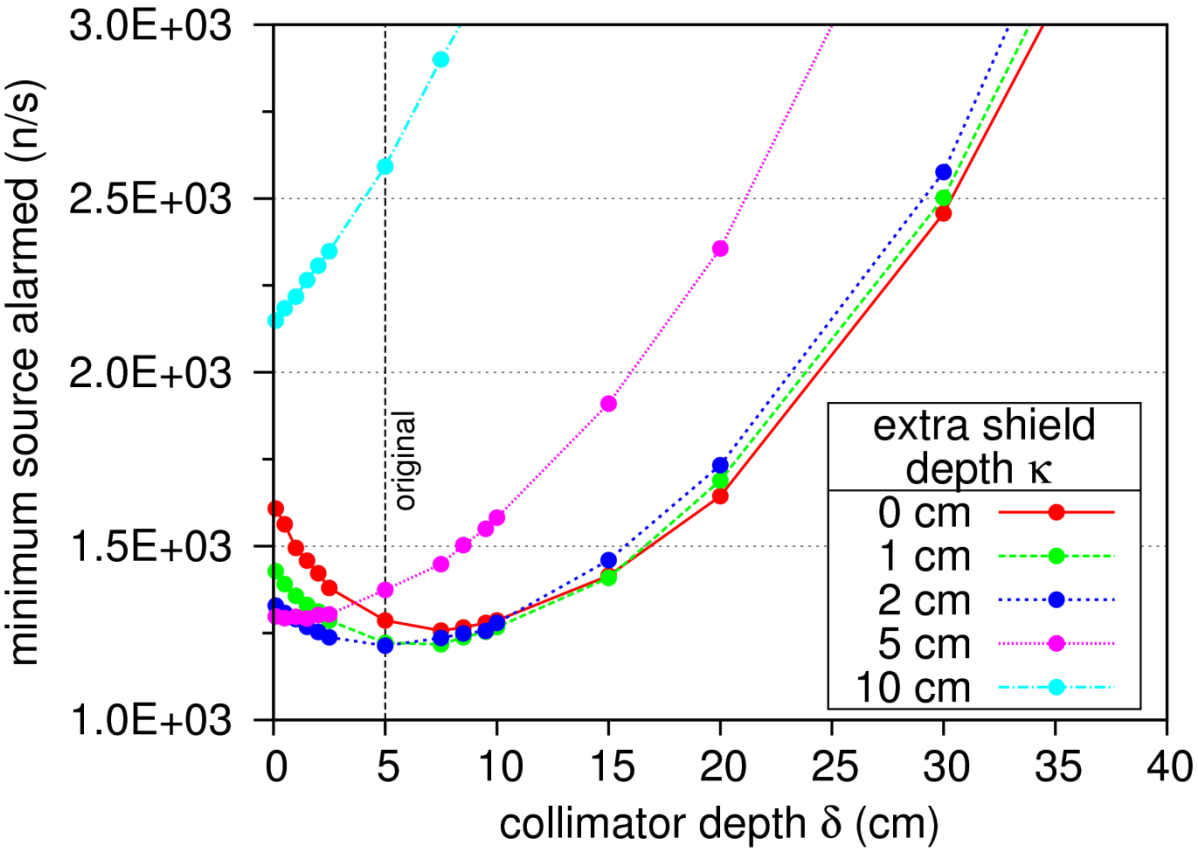


**Figure 11: Variation in minimum source alarmed as a function of collimator depth $\delta$ for different thicknesses $\kappa$ of extra forward shielding. The vertical line marked `original' represents the value of $\delta$ in the original study (Section 2), where $\kappa$ was 0.**

With $\kappa$ = 1 or 2 cm the results demonstrate that the original collimator thickness of 5 cm is still optimal producing a mean alarmed source of 1.2 x $10^3$ n/s, with $\kappa$ = 2 cm marginally better at this collimator depth. For this reason $\kappa$ = 2 was selected as the fixed forward shielding thickness in the remaining parameter study, where $\delta$, $o_r$ and $i_r$ are allowed to vary. This leads to a total of 4 cm between the edge of the stainless steel tanks enclosing the helium and the start of the collimator.

Figure 12 shows the variation in minimum alarmed source as a function of the ratio between $i_r$ and $o_r$ for different values of $\delta$, demonstrating that, almost without exception, keeping the holes in the collimator cylindrical is the best option. Note here that we are only considering a small subset of the collimator depths evaluated earlier because, as Figure 11 shows, the best detector efficiencies are obtained when $\delta$ is less than around 10 cm.

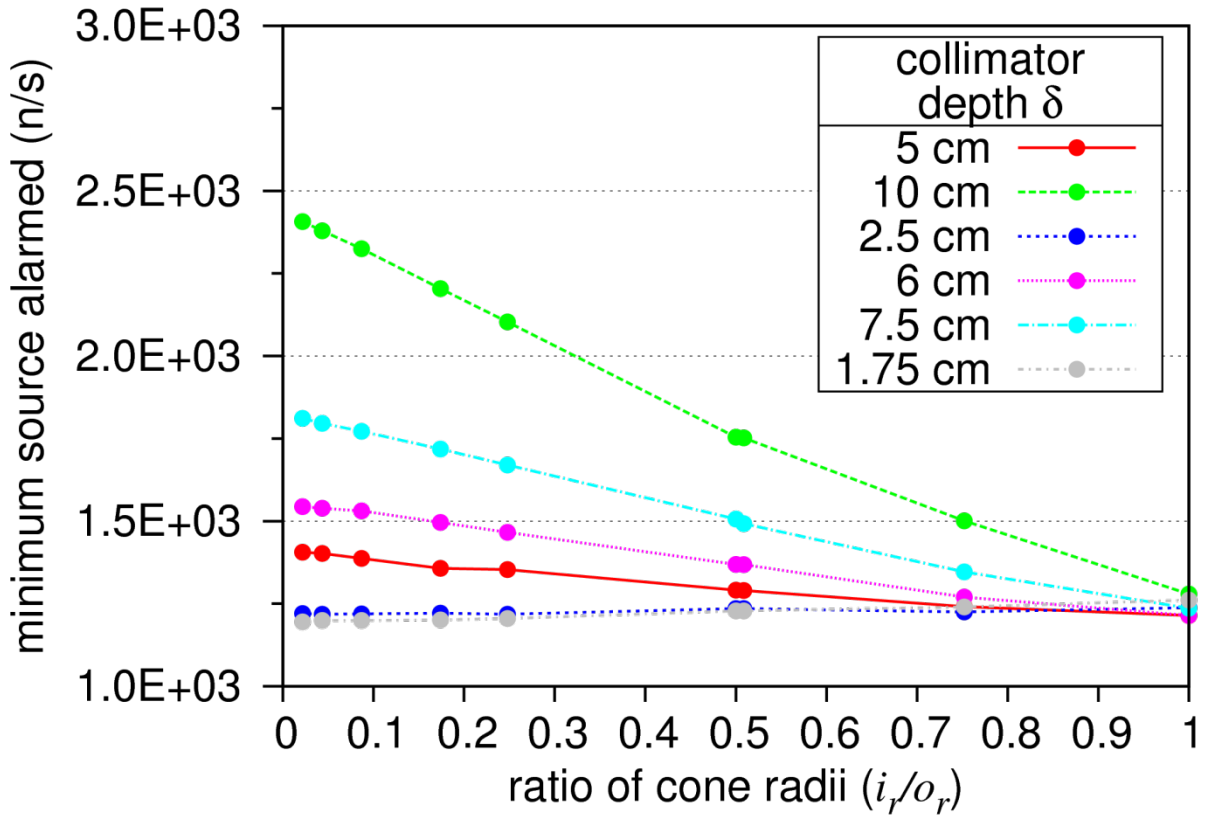


**Figure 12: variation in detector response as a function of the ratio of the inner or middle radius of the collimator holes to the outer radius. Curves are shown for different values of the collimator depth parameter $\delta$.**

For the very thinnest collimator configurations ($\delta$<2.5), there may be a very small benefit to having a more conical profile to the holes, but the minimum alarmed source remains ~1.2 × $10^3$ n/s in all cases. Since thin collimators have relatively little polythene to help with the attenuation of the neutrons, it is not surprising that any measure which increases the amount of material, such as tapering the holes, could produce improved detector performance. However, since a thicker collimator, such as the original 5 cm (red curve in the figure) from the preliminary study, can produce similar performance with cylindrical holes, it will be the cost-benefit balance that determines the best overall preference – i.e. is less boronated polythene with a complex lattice of gaps cheaper to make than using more polythene with simple drilled holes?

The final optimisation parameter considered was the packing density of the holes in the collimator themselves. Figure 13 shows the detector performance results as a function of the percentage of the front surface of the collimator (facing the threat) occupied by the holes, which, in the MCNP model, is controlled by varying $o_r$. In this case, the value of $i_r$ is kept equivalent to $o_r$, to maintain the optimum cylindrical hole profile. For all curves in the figure,

which represent different collimator depths, the lowest achievable alarmed source is once again 1.2 x $10^3$ n/s, which has been remarkably consistent throughout the parameter study. This possibly indicates that this is the lowest achievable result for the current choice of detector design – i.e. a fixed number of helium tubes with constant spacing – and threat type.

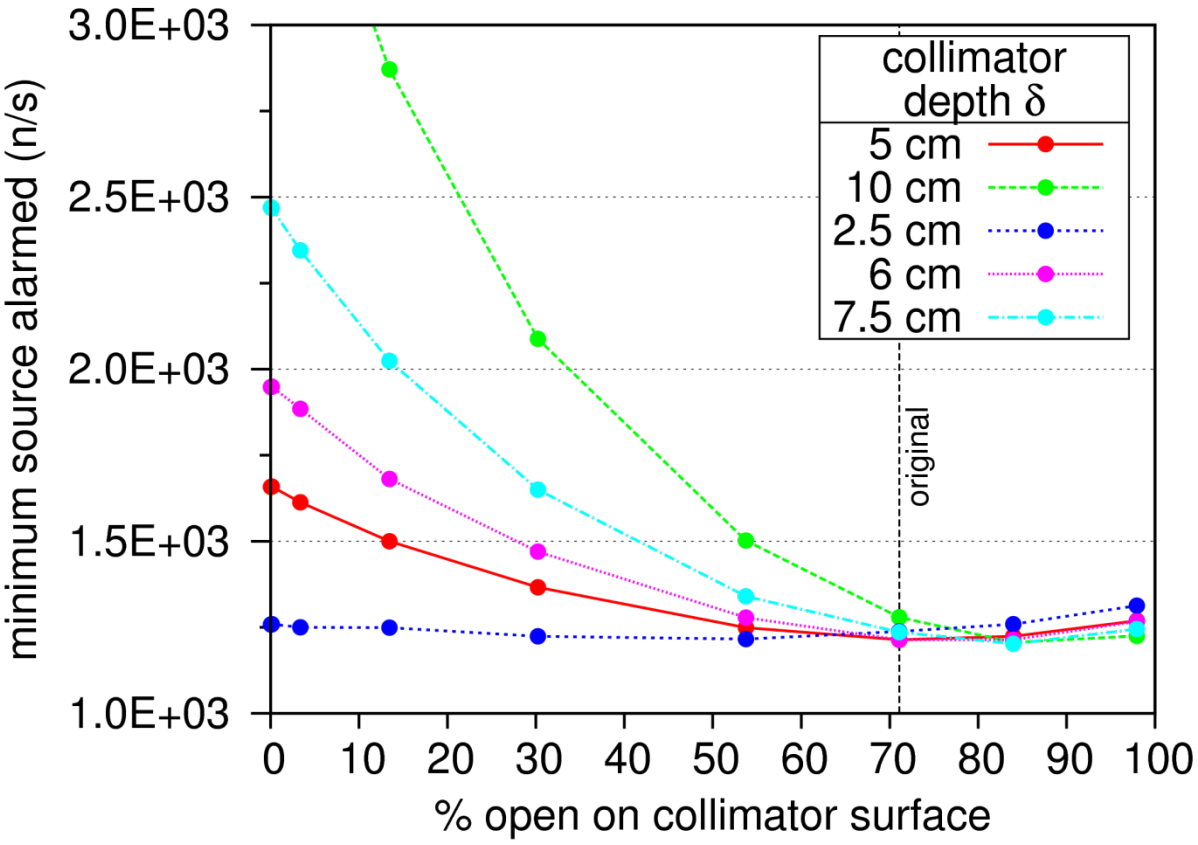


**Figure 13: variation in detector response as a function of the packing density of the collimator holes, measured as the percentage of (open) space occupied by the holes on the exposed face of the collimator, with boronated polythene making up the remainder. Curves are shown for various values of the collimator depth δ.**

The packing results in Figure 13, also demonstrate that the original design from the preliminary study, which has a packing percentage of 71% (vertical line in figure) and collimator depth of 5 cm, was close to optimum because this produces the minimum alarmed source, albeit with the 2 cm of extra shielding optimised previously. As before, for the very thinnest collimator designs, the optimum value of the other parameter, in this case $o_r$ is influenced by the need for more shielding. Thus for $\delta$ = 2.5 cm, a packing percentage of between 30-50%, i.e. more polythene, is optimum. For thicker collimators having smaller holes is significantly undesirable.

### *3.3 Optimisation summary*

In summary, for the parameter study, we find that an extra 2 cm thick polythene shield in front of the basic detector design improves response, and that additionally a collimator of depth 5 cm with cylindrical holes occupying about 70% of the exposed surface leads to a minimum source to alarm of 1.2 x $10^3$ n/s.

### *3.4 Base He-3 detector air gap optimisation*

Following advice from experts in the field of RPMs, we extended our study to include optimisation of the geometry of the detector units (helium tubes encased in polythene) themselves.

### 3.4.1 Model description

Preliminary simulations have shown that the inclusion of an air cavity surrounding a detector volume improves the response of a moderated He-3 detector to a simulated fission source. In order to optimise this affect a study has been carried out in order to identify the optimal moderator and air gap configuration for a single detector which leads to the greatest gain in signal response relative to that of a baseline model in the absence of an air cavity. The results of this work will then be used as a basis to further optimise the shielding and collimation of an array of He-3 detectors forming an RPM panel.

Two distinct detector geometries have been investigated:

- The detector volume surrounded by an air cavity consisting of a uniform cylindrical shell, Figure 14.
- The detector volume encompassed by a rectangular cuboid air-cavity, which is uniform around the detector volume, Figure 15.

Figures Figure 14 and Figure 15 show examples of geometry plots of the cylindrical shell cavity and the rectangular cuboid cavity, respectively. As can be seen from the images no background shielding was modelled nor was the ground modelled. The air cavity is shown in green, clearly surrounding the detector volume (in yellow). The polythene moderator/shielding material is shown in blue.

Air cavity optimisation simulations were carried out such that only a single detector element was modelled with reflecting boundaries, fixed at 6 cm either side of the centre of the detector. This allows for the simplified simulation of a bank of detectors with each detector element having a fixed width of 12 cm.

The mcnp_pstudy software tool [6] was used to automate the optimisation of the shielding and cavity design study using MCNP. The tool was used to create input decks by varying the geometric parameters defining the cavity size, the depth of polythene between source and detector and the depth of polythene on the far side of the detector relative to the source. These parameters were set to take the following range of values:

For the cylindrical shell cavity:

1. Cavity size:  2.52, 3, 3.5, 4, 4.5, 5, 5.5, and 6 cm.
2. Depth of polythene shielding on far side of detector (relative to source): 2.52, 4, 6, 8, and 10 cm.
3. Depth of polythene shielding on near side of detector 2.52, 4, 6, 8, and 10 cm.

For the rectangular cuboid cavity:

1. Cavity size:  2.52, 3, 3.5, 4, 4.5, 5, 5.5 and 6 cm.
2. Depth of polythene shielding on far side of detector (relative to source): 2.52, 4, 6, 8, 10, 12 and 14 cm.

3. Depth of polythene shielding on near side of detector 2.52, 4, 6, 8, 10, 12 and 14 cm.

The cavity here being the distance from the centre of the detector to the cavity surface and always extends from the base of the cylindrical detector to its top.

An extended Cf-252 Watt fission spectrum source term was simulated extending from -10 cm to 10 cm along the direction of the RPM, i.e. extending beyond the reflecting geometry; this source was biased to preferentially produce neutrons in the direction of the detector. The source to detector distance for the current optimisation was fixed at 100 cm and positioned 50 cm above ground level.

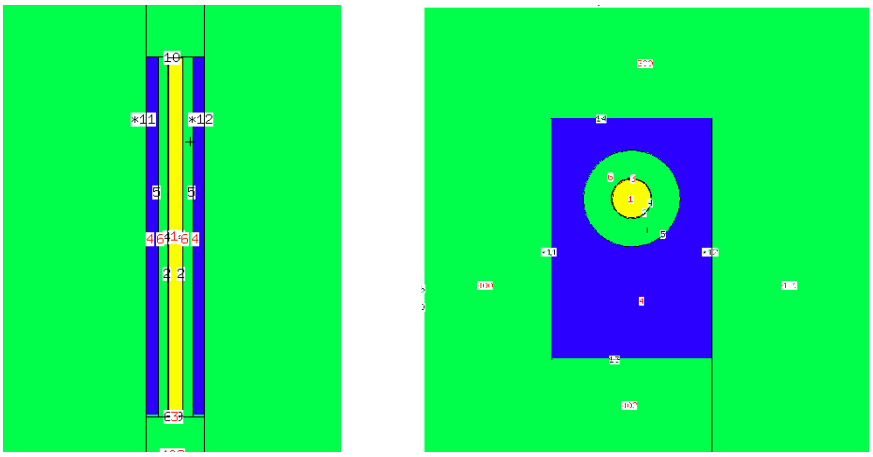

**Figure 14: Vertical (left) and horizontal (right) cross sections through the MCNP geometry, showing a simulated cylindrical shell air cavity (green) surrounded by polythene shielding (blue).**

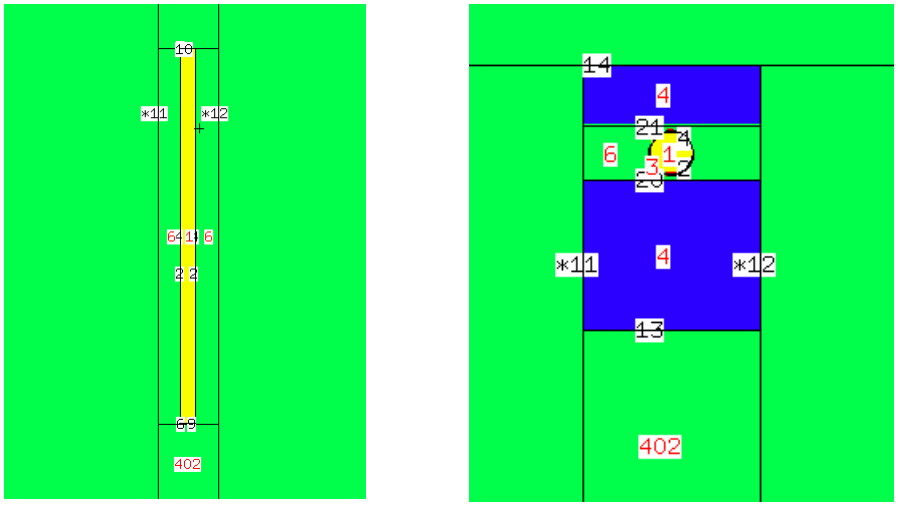


**Figure 15: Vertical (left) and horizontal (right) cross sections through the MCNP geometry, showing a simulated rectangular cuboid air cavity (green) surrounded by polythene shielding (blue). Reflecting boundaries are shown with asterisks.**

### 3.4.2 Results

The measure used to gauge the optimal detector response for this particular study was the He-3(n,p)H-3 reaction rate (RR) scored in the detector volume. The MCNP track length estimate of flux (F4 tally) was multiplied by the total and (n,p) cross section of He-3, thus resulting in a RR in arbitrary units. This response was scored in the detector volume for each parameter combination. 692 simulations were carried out in total; each running $1 \times 10^6$ particle histories, which resulted in better than 1% statistical uncertainty in almost every case. Any test cases with parameter combinations which resulted in overlapping geometry (i.e. geometry errors) between the air gap and the polythene shielding were rejected.

Through comparison of the results from the various geometries it was readily observable that the optimal cylindrical shell cavity, that with the highest RR, has an air gap of 4.5 cm with 8 cm polythene front shielding and 10cm polythene rear shielding. This configuration resulted in a RR of $3.61 \times 10^{-6}$ (rel. err. 0.006), a subset of results with 4.5 cm air gaps are shown in Table 2. The base line model, over which improvement is sought, having no air cavity and uniform 6 cm by 6 cm polyethylene shielding, resulted in a RR of $2.95 \times 10^{-6}$ (rel. err. 0.007). Thus the inclusion of a cylindrical shell air cavity and additional shielding resulted in an increase in reaction rate by a factor of 1.22.

**Table 2: Subset of parameter study results for the optimal air gap thickness in the cylindrical shell geometry.**

| Air gap [cm] | Rear Shielding [cm] | Front Shielding [cm] | Reaction Rate [arb. units] | Relative Error |
|---|---|---|---|---|
| 4.5 | 6 | 6 | 2.53E-06 | 0.008 |
| 4.5 | 8 | 6 | 3.2E-06 | 0.007 |
| 4.5 | 10 | 6 | 3.47E-06 | 0.006 |
| 4.5 | 6 | 8 | 2.86E-06 | 0.007 |
| 4.5 | 8 | 8 | 3.41E-06 | 0.006 |
| **4.5** | **10** | **8** | **3.61E-06** | **0.006** |
| 4.5 | 6 | 10 | 2.59E-06 | 0.007 |
| 4.5 | 8 | 10 | 2.99E-06 | 0.007 |
| 4.5 | 10 | 10 | 3.13E-06 | 0.007 |

**Table 3: Subset of parameter study results for the optimal air gap thickness in the rectangular cuboid geometry.**

| Air gap [cm] | Rear Shielding [cm] | Front Shielding [cm] | Reaction Rate [arb. units] | Relative Error |
|---|---|---|---|---|
| 3 | 12 | 4 | 1.88E-06 | 0.009 |
| 3 | 14 | 4 | 1.92E-06 | 0.008 |
| 3 | 12 | 6 | 3.02E-06 | 0.007 |

| | | | | |
|---|---|---|---|---|
| 3 | 14 | 6 | 3.04E-06 | 0.007 |
| 3 | 12 | 8 | 3.22E-06 | 0.007 |
| **3** | **14** | **8** | **3.23E-06** | **0.007** |
| 3 | 12 | 10 | 2.78E-06 | 0.007 |
| 3 | 14 | 10 | 2.80E-06 | 0.007 |
| 3 | 12 | 12 | 2.18E-06 | 0.008 |
| 3 | 14 | 12 | 2.19E-06 | 0.008 |
| 3 | 12 | 14 | 1.57E-06 | 0.009 |
| 3 | 14 | 14 | 1.57E-06 | 0.009 |

For the rectangular cuboid cavity simulations also showed an increase in RR over the baseline model, but not as significant as that for the cylindrical shell case. The optimal geometry having 3 cm air cavity and 8 cm polythene front shielding and 14 cm polythene rear shielding. Resulting in a RR of $3.23 \times 10^{-6}$ (rel. err. of 0.007) – a factor of 1.1 over the baseline case.

The optimal geometries for each configuration are shown relative to the baseline model in figure 5. It is interesting to note that the cross sectional area of the air gap is very similar between the two geometries, falling within approximately 10% of each other. Identical optimal distances from the front of the polythene shielding to the centre of the detector are also observed (8 cm), though the shape and thickness of this shielding differs between the models.

The spectra recorded in the detector volume, for each of the two optimal models and the base line model, are shown in Figure 16, all three spectra showing similar characteristics. The He-3 detector has a 1/v response and any optimal geometry will inevitably require a balance between thermalizing the fission spectra and retaining a high neutron flux to maximise detector response. From the spectra it can be seen that the optimal cylindrical shell air gap configuration has the highest thermal energy neutron flux per source neutron and thus, with contribution from the rest of the spectra, has the highest reaction rate. The optimal rectangular cuboid air gap also has a higher thermal neutron flux component than the base line model and thus a higher reaction rate.

Interestingly the higher energy flux peak shows the cylindrical shell air gap having a higher fast neutron component than the cuboidal geometry and suggests that the use of inelastic scattering materials in addition to the polythene moderator could help reduce the fast neutron energies further and improve detector response. The use of other moderator materials to improve the spectrum shaping is undoubtedly an approach worth pursuing but is beyond the scope of this work.

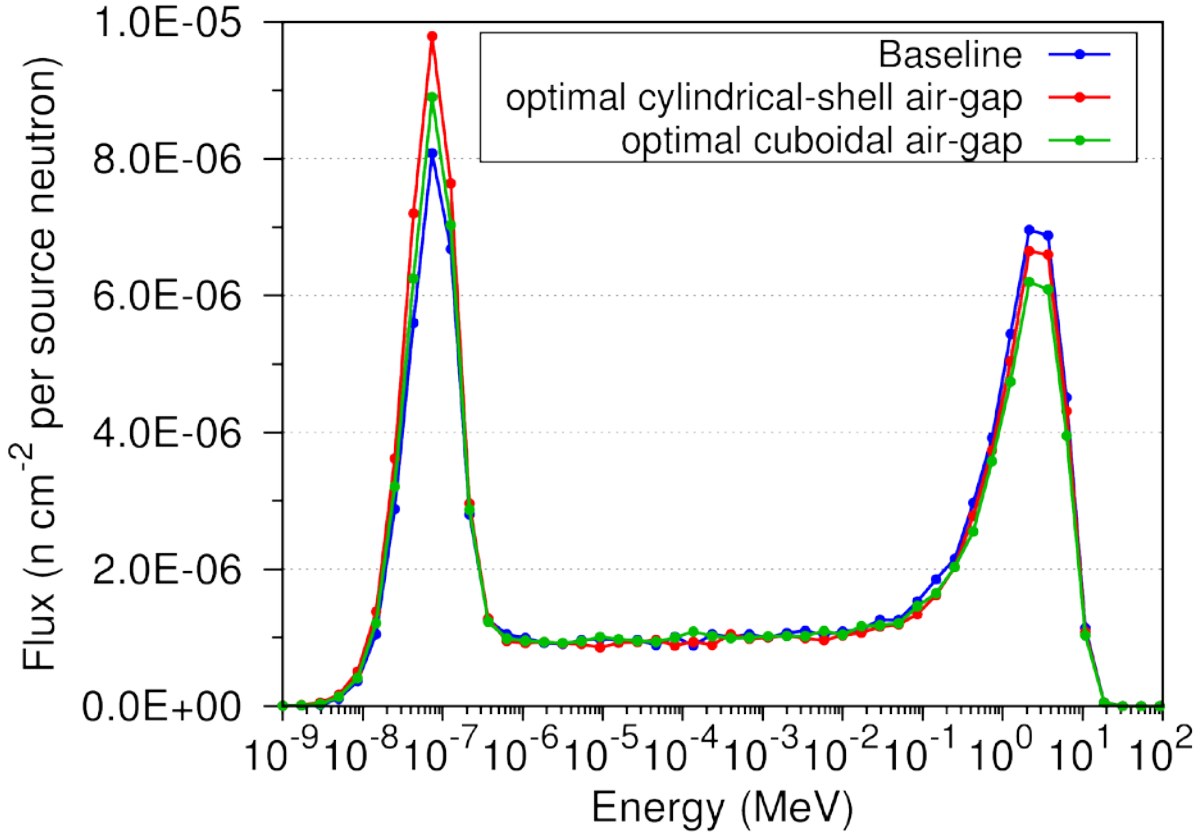


**Figure 16: Flux spectra recorded in the detector volume for the baseline and optimal detector configurations.**

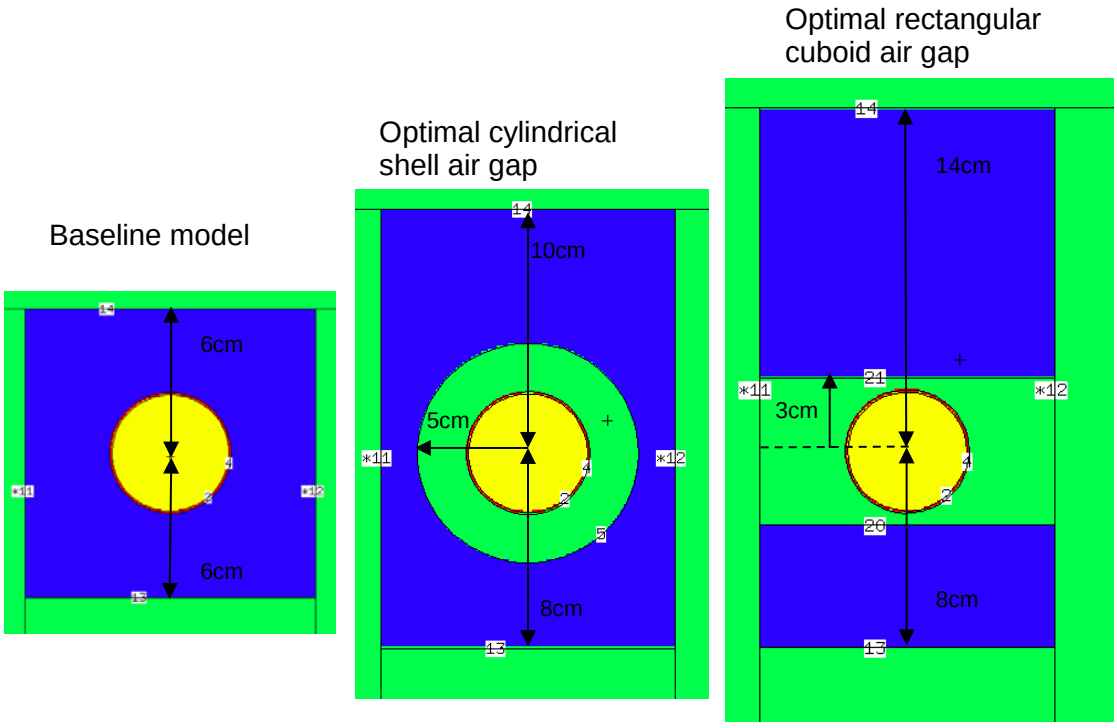


**Figure 17: Geometry plots of the baseline model (left), optimal cylindrical shell air gap (centre) and optimal rectangular cuboid air gap (right). Measurements show optimal polythene shielding thickness and air gap radius for the two parameter studies.**

### *3.5 Updated multi-parameter study using optimised base He-3 detector*

Following the optimisation of the basic detector design we now return to the optimisation of the shielding and collimator geometry. As before, we use the 'minimum source to alarm' measure to judge the relative effectiveness of different designs.

## 3.5.1 Model description

Rather than consider a basic detector design based on the exact findings of the base He-3 detector optimisation in the previous section, for this updated study we have simply taken the optimised cylindrical air cavity size of 4.5 cm, into which the standard He-3 tubes are positioned. This leads to a 1.98 cm thick shell of air surrounding the 2.52 cm radius tubes. The other variables regarding the thicknesses of the base polythene in front and behind the detector are considered as part of the optimisation process ($\kappa$ from section 3.2 already accounts for the front shielding).

Figure 18 shows the new design for optimisation, including the new variable $\lambda$ that controls the amount of extra polythene shielding between the helium tube units and the start of the rear boronated polythene shielding. As before, $\kappa$ varies between 0 and 10 cm in the study, while $\lambda$ can be up to 80 cm thick.

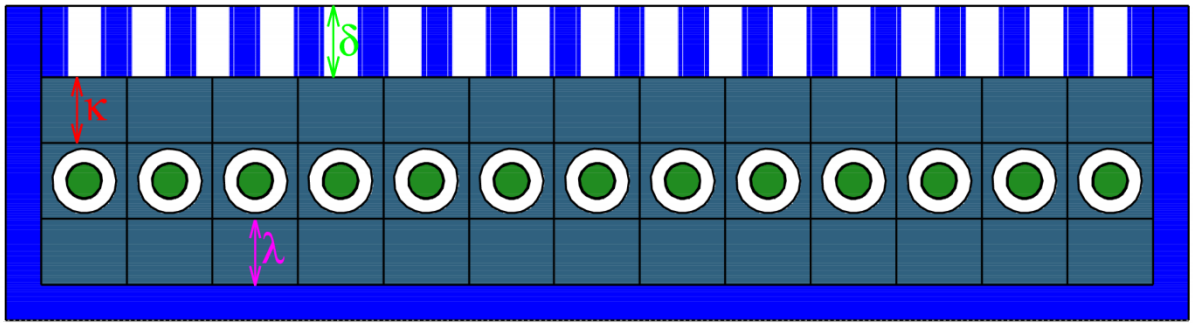


**Figure 18: Top view of detector showing additional optimisation parameter $\lambda$, which allows for extra polythene shielding behind the helium tubes. Note that in this new improved model the gap between the regions controlled by $\kappa$ and $\lambda$ and the edge of the air gap surrounding the helium tanks is only 0.02 cm (previously it was 2 cm when there was no air gap).**

## 3.5.2 Results

As in section 3.2, we considered the optimisation of the shielding thicknesses first, before allowing the other parameters to vary. Figure 19 shows a typical result from these simulations, in this case for a collimator depth of 5 cm. It is immediately apparent the best 'minimum source alarmed' has fallen from the $1.2 \times 10^3$ n/s observed in the initial parameter study, to around $1 \times 10^3$ n/s with the newly optimised helium tube unit cell and air gap – representing around a 15 % improvement in optimum performance.

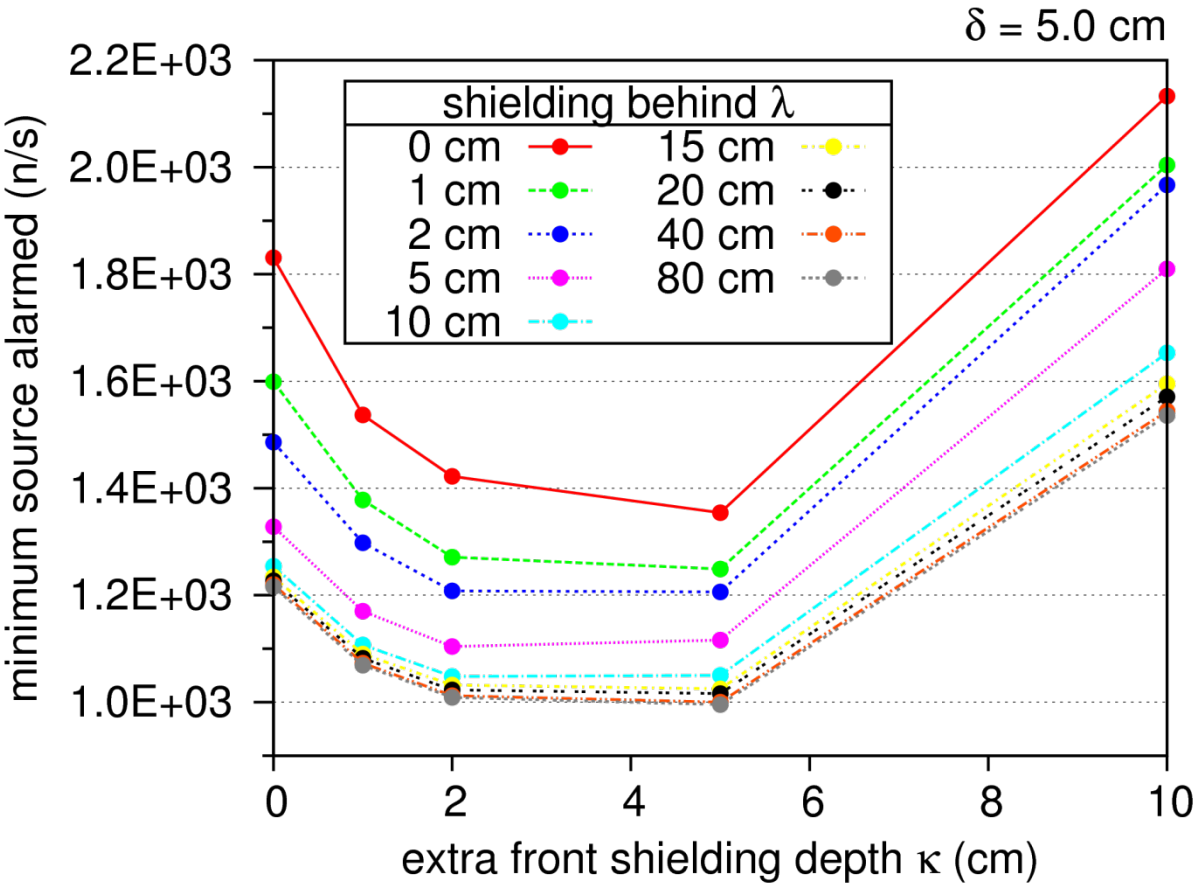


**Figure 19: Typical result from the extended parameter study showing the variation in response as a function of the solid shielding depths (κ and λ) for a fixed collimator depth of δ = 5 cm.**

Figure 19 also demonstrates that in general, the thicker the rear shielding the better – a result that is reproduced regardless of the collimator thickness δ. However, above about λ = 15 or 20 cm, there is only marginal improvement in detector performance, and so there is likely to be a trade-off with sensitivity versus cost of more polythene. In the remainder of the study we take λ = 40 cm as a mid-range thickness that gives almost optimum sensitivity.

In contrast to the previous parameter study, where κ = 2 was optimum, for the new geometry we find that it is an extra shielding thickness κ of 5 cm that produces the best detector performance. This reflects the fact that previously, where there was no air gap, there was already 2 cm of polythene between the helium tanks and the collimator before adding extra shielding through κ. Now, with the 4.5 cm radius air tube surrounding the tanks, the default shielding is virtually zero. Thus, it is not surprising that κ = 5 becomes optimum, and it is possible that κ = 4 might be slightly better still, although the 1 x $10^3$ n/s best minimum alarmed source is unlikely to change.

Using these optimised values of κ = 5 cm and λ = 40 cm, produces the simulation results shown in Figure 20 for the parameter study of the collimator profile. As before, there is no real benefit to making the holes more conical (ratio less than one in the figure), even when the collimator thickness is small.

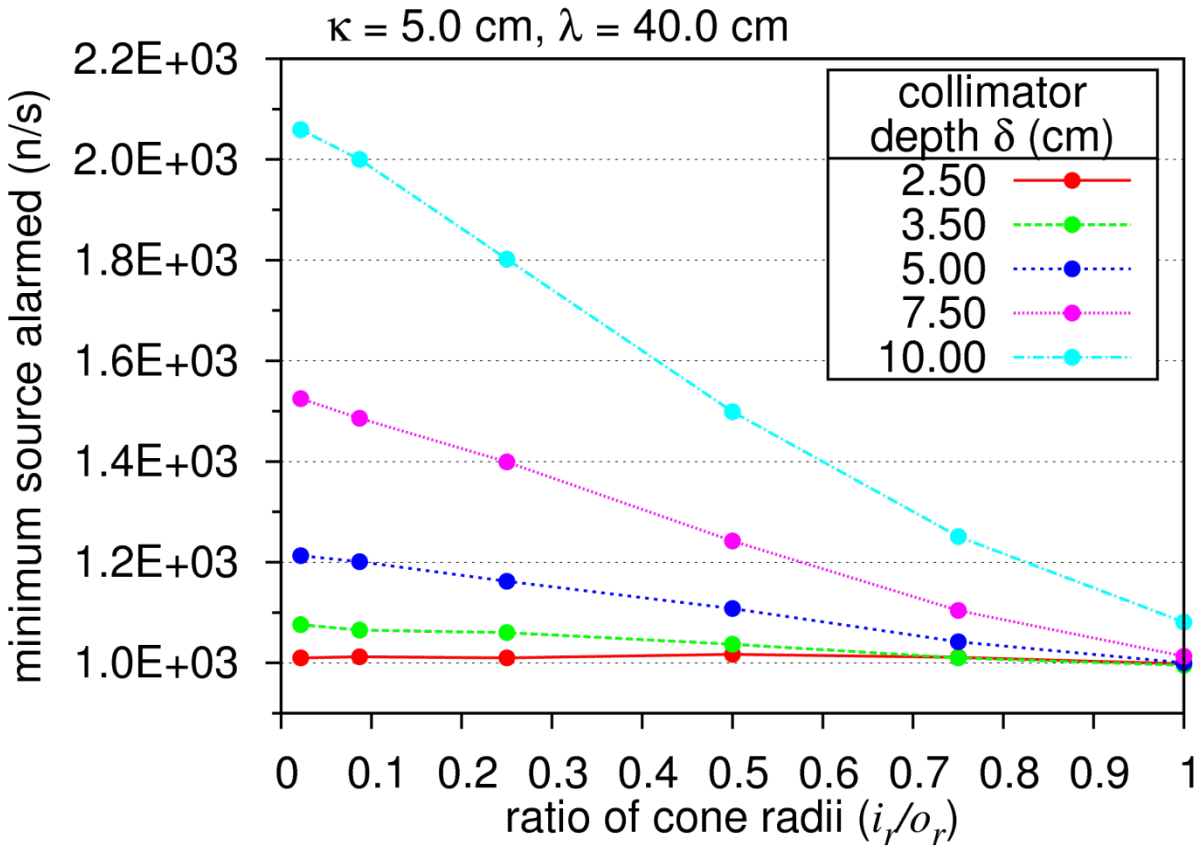


**Figure 20: Variation in minimum alarm level as a function of collimator profile for various values of δ. For the fixed optimised shielding thicknesses of κ and λ – as shown in the plot**

Note that, once again, δ = 5 cm produces a detector sensitivity that cannot be improved upon, further highlighting the fortuitous selection of this value in the preliminary study.

Finally, we vary the hole packing-density, producing the results in Figure 21, for the optimised values of κ and λ. The best minimum remains around 1000 n/s, but there is a slight benefit for some of the thicker collimators to having wider holes (greater % open in the plot).

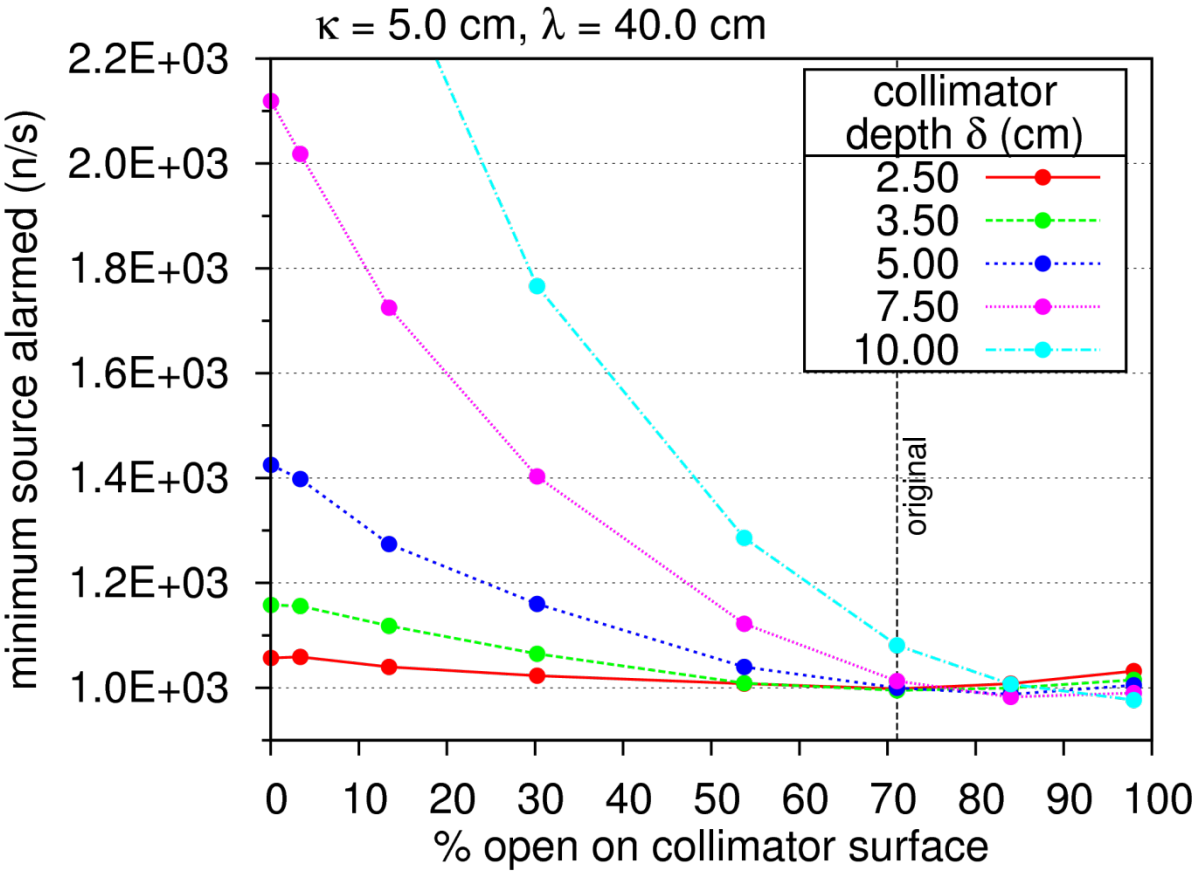


**Figure 21: Variation in minimum alarmed source as a function of cylindrical collimator hole packing density. Curves are shown for various values of the collimator depth parameter δ, but all for the same fixed values of κ and λ – as shown in the plot.**

## 4 SUMMARY AND DISCUSION

A series of design studies for a He-3-based radiation portal monitor (RPM) have been performed under a CLASP scheme funding grant. The sequence of studies, from a preliminary, 'proof of principle' investigation, through to detailed optimisations of the various shielding, collimator, and detector-design options, have built upon one-another and revealed via computational modelling that simple, cost-effective alterations to RPM design could produce significant improvements in sensitivity to threats present in a background neutron field.

The preliminary study demonstrated that adding both rear shielding and a simple collimator arrangement could significantly improve the response of a generic RPM design to a moving 'threat' source that in a realistic neutron background field. A parameter study for the collimator and additional forward shielding revealed that 2 cm of extra polythene in front of the detector improved performance. Together with a 5 cm thick collimator with cylindrical holes occupying around 70% of the exposed surface, this extra shielding (on top of the 5 cm thick rear shielding) could produce more than a factor of two improved sensitivity compared to the original, unmodified RPM. The optimised, modified RPM showed ~1200 n/s minimum threat detected compared to ~2600 n/s for the unmodified RPM.

Optimisation of the geometry immediately surrounding the He-3 tubes themselves indicated that the inclusion of an air gap, approximately 2 cm thick around the He-3 tubes improved the response of the detector to the threat source. Further optimisation of the shielding and collimator design for this new detector configuration produced a further 15% reduction in the `minimum source alarmed' performance measure (compared to the optimised configuration

with the original He-3 detector configuration). In particular, we observed that including thick shielding of 20 cm or more behind the detector reduced the response to the background while improving back-scattering of neutrons from the threat source. Combined with a 5 cm thick layer of forward shielding and the same 5 cm thick collimator with a exposed surface about 70% occupied by cylindrical holes, the sensitivity was improved sufficiently to detect a source strength of only 1000 n/s – a factor of ~2.6 improvement over the unmodified case.

## 5 RECOMMENDATIONS FOR FURTHER WORK

- During the optimisation studies it became apparent that a fully-fledged fitting program would be more efficient and would allow all parameters to vary at the same time. Work has already begun on this program, which would minimise the 'minimum source alarmed' objective function by varying the parameter set used to construct the MCNP model. The resulting 'best parameter set' is expected to reveal be a more precise optimum than those discussed so far.
- The current studies were restricted to He-3 detectors and an unshielded $^{252}$Cf neutron source threat. Further studies should investigate the variation in optimum parameters for both different detectors, such as $^{6}$Li-based scintillators or other non-He-3 based technologies, and different threat types, including shielded sources and different spectral sources such as $^{241}$Am-Be, $^{241}$Am-Li, fissile metals and oxides for example. In addition, sensitivity of optimum configurations to changing background level and exotic shield/collimation materials would be of interest to demonstrate robustness of design.
- Experimental feasibility study and/or activity to investigate and/or demonstrate improvements using a prototype shield and collimator back-fitted to an existing RPM.

## ACKNOWLEDGEMENTS

The authors would like to thank Dick Lacey of the Home Office Scientific Development Branch for useful discussions in support of this work. This work was funded under the CLASP research grant STK000152/1.

## 6 REFERENCES

[1] V O'Shea, J McMillan, L W Packer, CLASP proposal, optimising the neutron radiation environment of radiation portal monitors, Jan 2012.

[2] MCNPX version 2.7a manual.

[3] Version 2.22 developed by T. Sato, see T Sato and K Niita, Analytical Functions to Predict Cosmic-Ray Neutron Spectra in the Atmosphere, Rad. Res. **166** (2006) 544

[4] R.T. Kouzes et al., Passive neutron detection for interdiction of nuclear material at borders, Nuclear Instruments and Methods in Physics Research A **584** (2008) 383.

[5] L. A. Currie, Limits for Qualitative Detection and Quantitative Determination: Application to Radiochemisty, Anal. Chem. **40** (1968) 587.

[6] F. B. Brown, J. E. Sweezy and R. B. Hayes. Monte Carlo Parameter Studies and Uncertainty Analysis with MCNP5. PHYSOR-2004, American Nuclear Society Reactor Physics Topical Meeting, April 25-29, 2004.